DOI: 10.1002/ejic.200700986

Synthesis of Nanocrystalline Iron Oxide Particles in the Iron(III) Acetate/Alcohol/Acetic Acid System

Marijan Gotić*[a] and Svetozar Musić[a]

Keywords: Acetates / Magnetite / Hematite / Esterification / Solvothermal synthesis

Nanosized iron oxide particles were synthesised without the addition of water by autoclaving iron(III) acetate/alcohol and iron(III) acetate/acetic acid/alcohol solutions at 180 °C for different time periods. Magnetite was formed in iron(III) acetate/ethanol, whereas hematite was formed in the iron(III) acetate/acetic acid/ethanol system. The average crystallite sizes of 11.1 and 22.6 nm and the stoichiometry of $Fe_{2.89}O_4$ were found for the nanosized magnetite particles. The primary magnetite particles aggregated into regular spheres 5 to 10 μm in size, which can be explained by the specific character of the small, reactive and polar molecules of ethanol. In the iron(III) acetate/octanol system, a mixture of magnetite and hematite was obtained. The average crystallite size of magnetite was up to 22 nm and that of hematite was up to 46.7 nm. In the iron(III) acetate/acetic acid/ethanol system, nanosized hematite particles were exclusively formed. ^{13}C NMR spectroscopy revealed the presence of ethyl acetate ester in the supernatants. The formation of ester in the iron(III) acetate/ethanol system was explained by the catalytic oxidation of ethanol in the presence of acetate groups bonded to iron. Thus, in the oxidative dehydrogenation of ethanol into ethyl acetate, coordinated Fe^{3+} served as an electron acceptor that was reduced to Fe^{2+}, and exclusively magnetite was formed. With the addition of acetic acid to the iron(III) acetate/ethanol system, the free acetic acid directly participated in an esterification reaction with ethanol. Water molecules generated in situ in this esterification reaction hydrolysed iron(III) acetate, and thus hematite was formed.

Introduction

Metal oxide particles have found important applications as pigments and fillers, catalysts, gas sensors, magnetic materials and so on. Knowledge of the correlation between the synthetic conditions of specific metal oxide and its functional properties is important in obtaining material for possible applications in advanced technologies. For this reason, new synthetic routes for obtaining metal oxides have been extensively investigated. The traditional solid-state routes that involve the direct reaction of a mixture of powders[1a] or the thermal decomposition of various organic precursors[1b] are two of the routes available in the synthesis of metal oxide powders. However, the solid-state reaction is inflexible and requires high temperatures, and it is difficult to control the properties of the particles. In contrast, solution-based or "wet" chemistry synthesis offers very good control over particle size, morphology and phase composition of the final product; hence, the syntheses can be performed exclusively in aqueous[2a,2b] or organic media.[2c] Recently, nanosized magnetite particles were synthesised by using a γ-irradiated water-in-oil microemulsion.[2e] The γ irradiation created strong reductive conditions in the microemulsion so that magnetite was formed even though the synthesis started from a pure iron(III) precursor ($FeCl_3$).[2d] The precipitation of the corresponding salts from solution,[2e] forced hydrolysis, hydrothermal,[3a] hydrothermal in near-supercritical water,[3b] sol–gel,[3c–3f] polyol[4] and nonhydrolytic syntheses[5a–5c] are also "wet" chemistry routes often utilised in the synthesis of metal oxide particles. The sol–gel route is one of the most exploited synthetic routes, because it provides excellent control of physical, chemical and microstructural properties at the molecular level. It allows advanced materials to be obtained in a wide variety of physical forms such as fibres, films, coatings, composites, sols, gels, powders, monoliths and membranes. Metal alkoxides are usually starting precursors in the sol–gel synthesis; however, some of them are very sensitive to moisture and show a high hydrolysis rate and uncontrolled precipitation upon the addition of water. In a previous paper, we showed that nanosized TiO_2,[6a] V_2O_5 (unpublished results), Bi_2O_3[2e] and Fe–TiO_2 nanoparticles[6b,6c] can be successfully synthesised by using an esterification reaction between acetic acid and an alcohol. In this route, a metal cation was homogeneously hydrolysed by slowly released water molecules generated in situ as follows: $CH_3COOH + ROH \rightarrow CH_3COOR + H_2O$. By using this approach, the reactivity of the metal alkoxide precursor as well as the hydrolysis rate were accurately controlled.

In this paper, we present new results relating to the synthesis of nanosized iron oxide particles by using the esterifi-

[a] Ruđer Bošković Institute,
Bijenička 54, Zagreb 10000, Croatia
Fax: +385-1-4561-123
E-mail: gotic@irb.hr

cation reaction in the iron(III)/acetic acid/alcohol system. The synthesis started from a clear iron(III) organic solution that was stable at room temperature for months. However, at elevated temperatures and under the pressure of the autoclave, a nanocrystalline iron oxide phase(s) was obtained. Control of the phase composition, morphology, aggregation and particle size of the obtained iron oxides was achieved by adjusting experimental parameters such as the type of alcohol, the molar ratio of iron(III)/acetic acid/alcohol and the temperature. The "pure" systems without added acetic acid, iron(III) acetate/ethanol and iron(III) acetate/octanol were also studied.

Results and Discussion

Figure 1 shows field emission scanning-electron microscope (FE SEM) micrographs of samples ET1, ET2 and ET3 obtained by dissolving iron(III) acetate in ethanol after the solution was autoclaved at 180 °C for 2, 8 and 16 h, respectively. Figure 1a (sample ET1) shows particles aggregated into compact regular spheres (secondary particles), and Figure 1a′ is a magnified image showing discrete particles (primary particles) on the surface of one sphere. When the sample was autoclaved for 8 h (sample ET2), particles arranged in regular spheres were still produced; however, some of them were "scratched". Figure 1 b′ shows a "scratched" particle at higher magnification. After the sample was autoclaved for 16 h (sample ET3), secondary particles were visible as irregular spheres. These particles are less compact, so primary particles are clearly visible at lower (Figure 1c) and at higher magnification (Figure 1c′).

Figure 2 shows the room-temperature Mössbauer spectra of samples ET1 and ET3 and stoichiometric magnetite ($Fe_{3.00}O_4$) for comparison. Stoichiometric magnetite was obtained by hydrogenation of a commercial substoichiometric magnetite ($Fe_{2.90}O_4$) containing about 7.0 wt.-% of α-Fe_2O_3 as an impurity. The room-temperature Mössbauer spectrum of these micrometre-sized stoichiometric $Fe_{3.00}O_4$ particles can be fitted with two sextets. The outer sextet has a hyperfine magnetic field B_{hf} = 48.9 T and the isomer shift δ = 0.28 mm s^{-1} relative to α-Fe, and it corresponds to the Fe_A^{3+} ions at the tetrahedral A sites. The inner sextet has B_{hf} = 45.8 T and δ = 0.67 mm s^{-1}, and it is due to the Fe^{2+} and Fe^{3+} ions at the octahedral B site. Because the Fe_B^{2+} and Fe_B^{3+} sites are indistinguishable at room temperature due to the rapid electron-hopping process, which is faster ($\tau \approx 1$ ns) than the decay of the excited state of ^{57}Fe ($\tau \approx$ 98 ns), the inner sextet is fitted to the average charged $Fe_B^{2.5+}$. The nonstoichiometry of magnetite could be measured by a decrease in the relative surface area of the inner sextet in the Mössbauer spectrum. Besides the stoichiometry, the particle size also has a strong influence on the Mössbauer parameters, because magnetically ordered materials in the form of very small particles exhibit superparamagnetic behaviour. The superparamagnetic nanosized magnetite particles (smaller than 10 nm) show a doublet in the Mössbauer spectrum at room temperature. In the inter-

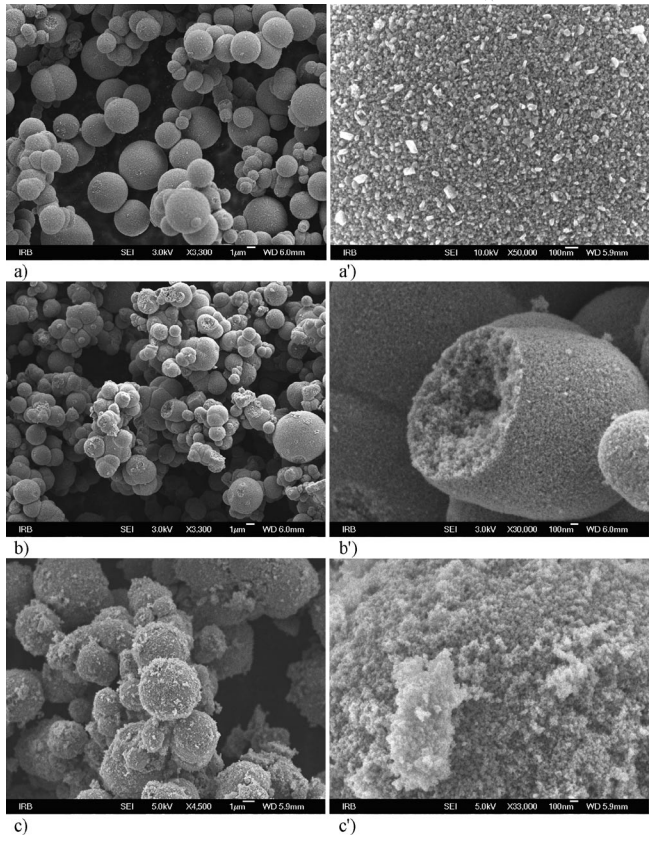

Figure 1. (a) FE SEM micrographs of sample ET1 and (a′) an enlarged section showing discrete particles on the surface of one sphere; (b) sample ET2 and (b′) an enlarged section showing the "scratched" particles completely consisting of smaller nanosize particles; (c) sample ET3 and (c′) an enlarged section showing nanosized discrete particles.

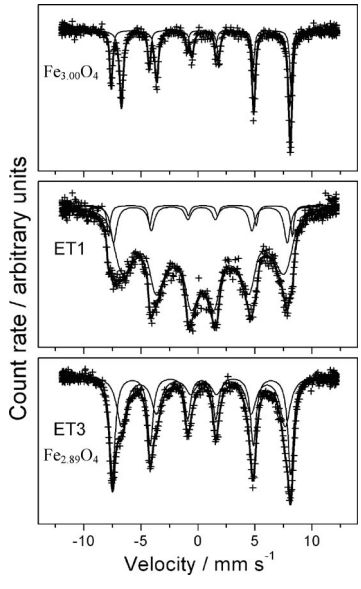

Figure 2. ^{57}Fe Mössbauer spectra of stoichiometric magnetite ($Fe_{3.00}O_4$) and samples ET1 and ET3, recorded at room temperature. Stoichiometric magnetite was obtained upon hydrogenation of commercial substoichiometric magnetite.

Table 1. ^{57}Fe Mössbauer parameters at room temperature calculated for stoichiometric $Fe_{3.00}O_4$ and samples ET1 and ET3.[a]

Sample	Fitting procedure	δ / mm s^{-1}	Δ or E_Q / mm s^{-1}	B_{hf} / T	Γ / mm s^{-1}	Area / %	Phase composition	Phase fraction
Fe_3O_4	M1	0.28	–0.03	48.87	0.27	34.3	Magnetite ($Fe_{3.00}O_4$)	1.00
	M2	0.67	0.02	45.79	0.38	65.7		
ET1	M1	0.26	–0.11	47.24	0.64	10.7	Magnetite (substoichiometric)	0.95
	$M2_D$	0.44	0.08	33.1	1.07	84.6		
	H1	0.33	–0.23	49.96	0.34	4.7	Hematite	0.05
ET3	M1	0.32	–0.02	48.49	0.60	53.6	Magnetite ($Fe_{2.89}O_4$)	1.00
	M2	0.49	–0.02	44.50	1.06	34.5		

[a] δ = isomer shift given relative to α-Fe at room temp.; Δ or E_Q = quadrupole splitting; B_{hf} = hyperfine magnetic field; Γ = line width. Error: δ = ±0.01 mm s^{-1}; Δ or E_Q = ±0.01 mm s^{-1}; B_{hf} = ±0.2 T. PD = paramagnetic doublet; $M2_D$ = subsextet fitted to the distribution of hyperfine magnetic fields; M1 = outer subsextet of magnetite; M2 = inner subsextet of magnetite; H1 = sextet of hematite.

mediate range (magnetite particle size about 10–20 nm), complex Mössbauer spectra with broadened lines and unusual line shapes are formed at room temperature.[2c] The Mössbauer spectrum of sample ET1 is fitted to three subsextets, H1, M1 and M2 (Table 1). The H1 subsextet has the highest value of hyperfine magnetic field and corresponds to hematite. The M1 subsextet corresponds to the outer subsextet of magnetite, whereas the M2 collapsing subsextet, which is fitted to the distribution of hyperfine magnetic fields, corresponds to the inner sextet of magnetite. Broadened lines and the collapsing nature of the inner subsextet are the net effects of small particle size, crystal defects and a general poor stoichiometry. The Mössbauer spectrum of sample ET3 is typical of nonstoichiometric magnetite. The ratio of the surface areas of the inner and outer subsextet gives the stoichiometry of $Fe_{2.89}O_4$ (Table 1).

Figure 3 shows the results of Rietveld analysis for samples ET1, ET2 and ET3. XRD patterns of sample ET1 perfectly matched the patterns of hematite (JCPDS 33–664) and magnetite (JCPDS 19-629). The XRD patterns of samples ET2 and ET3 consisted of magnetite as the only present oxide phase. Rietveld analysis gave average crystallite sizes of 11.1, 13.8 and 22.6 nm for magnetite in sample ET1, ET2 and ET3, respectively. The calculated weight fraction of hematite in sample ET1 is 0.09, and the average crystallite size of hematite is 36.6 nm.

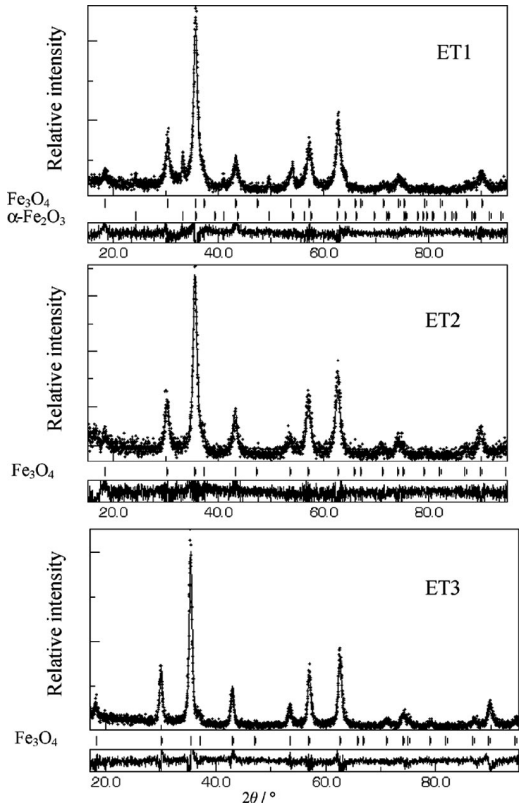

Figure 3. Rietveld refinement plot of samples ET1, ET2 and ET3. Experimental data are indicated by crosses, whereas the calculated curve obtained after the refinement is indicated with a continuous line. The upper tick marks in sample ET1 correspond to magnetite and the lower tick marks correspond to hematite. The continuous curve under the tick marks represents the difference between the experimental data and the calculated curve.

Figure 4 shows FE SEM micrographs of a sample obtained in the iron(III) acetate/octanol system. Sample OC1 consists of very small particles aggregated in an irregular region and of bigger discrete particles (≈ 30 nm) in the vicinity. Samples OC2 and OC3 consist of two types of discrete particles. With a prolonged autoclaving time, the size of the particles increases and the cloudy region is transformed into discrete particles that are suitably visible in samples OC2 and OC3.

Figure 5 shows the Mössbauer spectra of samples OC0 to OC3. Sample OC0 is characterised by a doublet and collapsing sextets. If the samples were autoclaved for longer times (samples OC1 to OC3), substoichiometric magnetite and hematite were obtained. Substoichiometric magnetite is characterised by two sextets (discussed previously in the text), and hematite has one sextet with the highest value of the hyperfine magnetic field. Mössbauer parameters for these samples are given in Table 2. With increased times of autoclaving, the relative amount of hematite decreased, whereas the hyperfine magnetic field shifted to higher values, which thus suggests better crystallinity. However, magnetite as a single phase was not obtained. According to Rietveld analysis (results not shown), samples OC1 to OC3 consisted of nanostructured magnetite and hematite. The average crystallite size of magnetite increased from 14.5 to 22.0 nm, and that of hematite from 30.6 to 46.7 nm. The relative concentration of hematite decreased from 30.0 wt.-

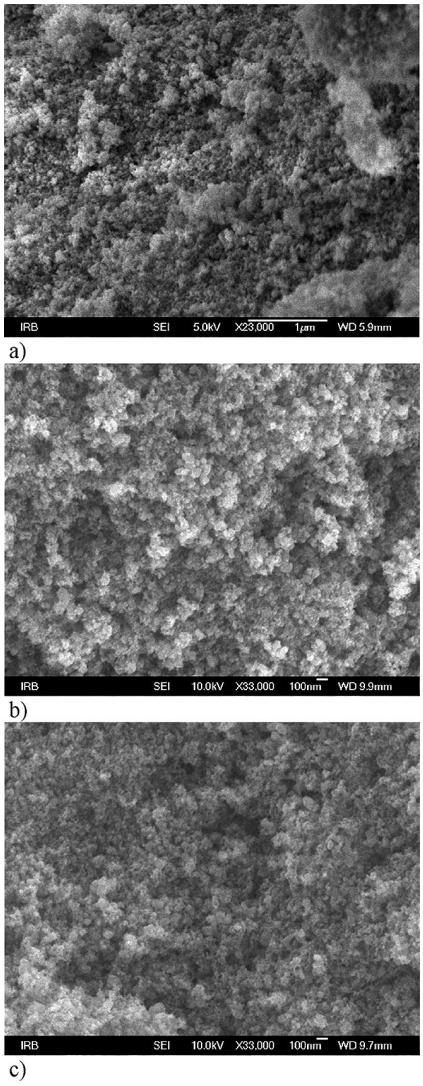

Figure 4. FE SEM micrographs of samples (a) OC1, (b) OC2 and (c) OC3.

% in sample OC1 to 20.4 wt.-% in sample OC3. Mössbauer spectroscopy gave a smaller relative concentration of hematite in comparison to that obtained by Rietveld analysis. This quantitative difference is due to different fitting procedures and similar parameters of the hyperfine magnetic field for hematite and the outer sextet (M1) of magnetite. These two sextets could overlap in the case of small particle sizes and low crystallinity of hematite.

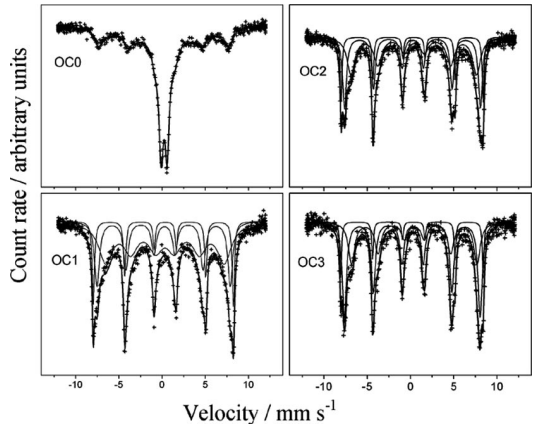

Figure 5. Room-temperature ^{57}Fe Mössbauer spectra of samples OC0, OC1, OC2 and OC3.

Figure 6 shows the FE SEM micrographs of nanosized particles formed in the iron(III) acetate/acetic acid/ethanol system (samples AC1, AC2 and AC3). At a low content of acetic acid (AC1), three completely different morphologies are visible: particles in the form of regular large spheres, small discrete particles of about 80–100 nm and cloudy regions with no visible discrete particles. At a higher acetic acid content (AC2), only discrete particles of irregular shape and cloudy regions are visible. There is no secondary aggregation into spheres. At the same content of acetic acid but with longer autoclave times (AC3), rather uniform pseudospherical particles without cloudy regions are visible.

Figure 7 shows the Mössbauer spectra of the same series of samples. The Mössbauer spectrum of sample AC1 is fitted to the paramagnetic doublet (superparamagnetic particles), subsextets M1 and M2, which correspond to substoichiometric magnetite, and to sextet H1, which corresponds to hematite. The inner subsextet M2 of magnetite has a low

Table 2. ^{57}Fe Mössbauer parameters calculated for samples OC0 to OC3 at room temperature.[a]

Sample	Fitting procedure	δ / mm s^{-1}	Δ or E_Q / mm s^{-1}	B_{hf} / T	Γ / mm s^{-1}	Area / %	Phase composition	Phase fraction
OC0	PD	0.24	0.67		0.63	41.1		0.41
	M_D	0.24	–0.15	37.75	0.94	58.9	Magnetite or maghemite	0.59
OC1	M1	0.23	–0.10	47.84	0.68	30.0	Magnetite	0.84
	M2	0.34	–0.00	42.55	1.96	53.8	(substoichiometric)	
	H1	0.26	–0.22	50.25	0.31	16.2	Hematite	0.16
OC2	M1	0.24	–0.03	48.75	0.54	41.0	Magnetite	0.83
	M2	0.40	–0.05	45.01	1.08	42.0	(substoichiometric)	
	H1	0.29	–0.22	50.96	0.26	16.9	Hematite	0.17
OC3	M1	0.22	–0.04	48.69	0.58	53.8	Magnetite	0.88
	M2	0.44	–0.01	45.02	0.87	34.5	($Fe_{2.85}O_4$)	
	H1	0.26	–0.21	51.11	0.24	11.7	Hematite	0.12

[a] δ = isomer shift given relative to α-Fe at room temp.; Δ or E_Q = quadrupole splitting; B_{hf} = hyperfine magnetic field; Γ = line width. Error: δ = ±0.01 mm s^{-1}; Δ or E_Q = ±0.01 mm s^{-1}; B_{hf} = ±0.2 T. PD = paramagnetic doublet; M_D = sextet fitted to the distribution of hyperfine magnetic fields; M1 = outer subsextet of magnetite; M2 = inner subsextet of magnetite; H1 = sextet of hematite.

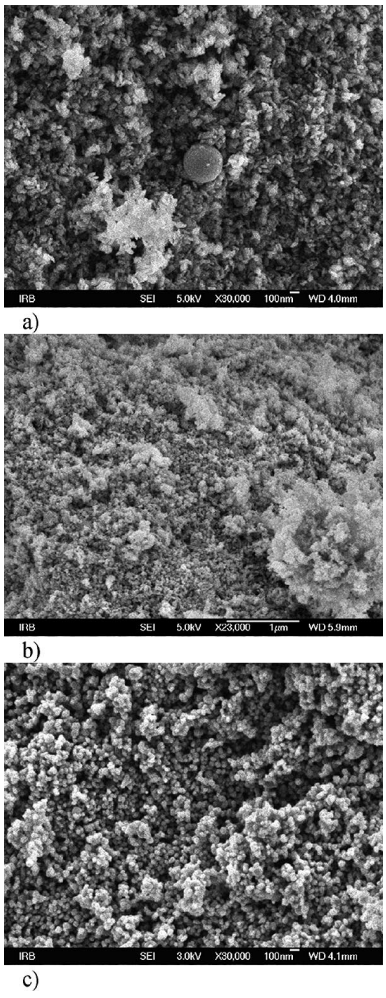

Figure 6. FE SEM micrographs of sample (a) AC1, (b) AC2 and (c) AC3.

value of the hyperfine magnetic field (43.17 T) and very broad spectral lines (1.61 mm s^{-1}). This can be explained by the addition of acetic acid (5 mL) and a short autoclaving time (2 h). At a higher concentration of acetic acid (12.5 mL), an additional disorder effect was introduced, so that the inner subsextet M2 of magnetite in sample AC2 was fitted to the distribution of the hyperfine magnetic field. A broad singlet ("smear singlet") was additionally introduced in order to remedy the higher disorder and to obtain a satisfying fit. The stoichiometry of magnetite for samples AC1 and AC2 is not possible to calculate as a result of the very broad spectral lines of the M2 subsextet. The Mössbauer spectrum of sample AC3 (the same conditions as those used for sample AC2 but with an autoclave time of 24 h) corresponds to pure hematite having B_{hf} = 50.84 T. A very small fraction of the "smear doublet" (2.3%) was introduced to obtain a better fit. The relative amount of hematite increased with the addition of acetic acid (15 and 18 mol-% for samples AC1 and AC2, respectively). Furthermore, in the presence of acetic acid and after a prolonged autoclave time hematite was present as a single phase.

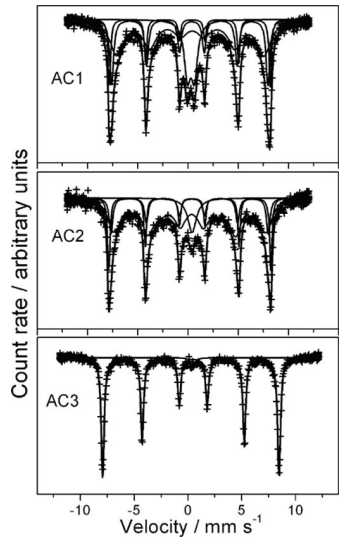

Figure 7. Room-temperature ^{57}Fe Mössbauer spectra of samples AC1, AC2 and AC3.

Figure 8 shows the FE SEM micrographs of samples obtained in a diluted iron(III) acetate (0.1 g)/acetic acid (8.5 mL)/ethanol (16.5 mL) system (sample AD1). Characterisation of this sample by using Mössbauer spectroscopy showed that it consisted of hematite as a single phase. The same sample obtained from a different iron acetate source (sample AD2, results not shown) possessed the same phase composition and virtually the same rhombohedral mor-

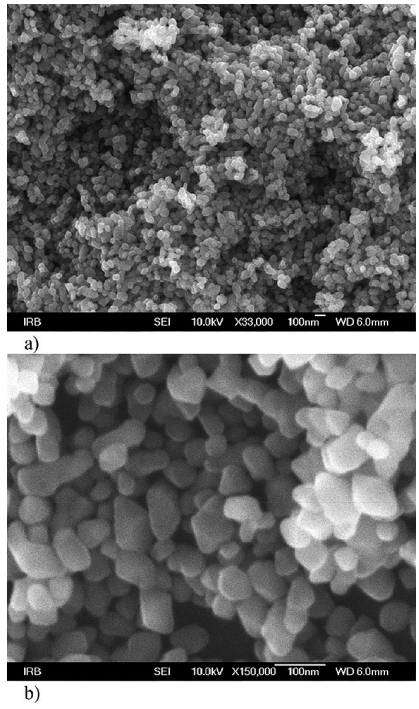

Figure 8. FE SEM micrograph of a sample in a diluted iron(III) acetate (0.1 g)/acetic acid (17 mL)/ethanol (33 mL) system (sample AD1) obtained at (a) low magnification and (b) at high magnification.

phology of the particles, which thus confirmed the reproducibility of the results, regardless of the manufacturer of the starting chemical.

Figure 9 shows the ^{13}C NMR spectra of selected samples studied in this work. Figure 9a shows the ^{13}C NMR spectrum of a solution of iron(III) acetate (0.1 g) in the presence of ethanol (17 mL) and acetic acid (33 mL). The solution was aged for 3 months at room temperature, but there was no precipitate. The peaks at 14.9 ($CH_3COOCH_2\mathit{C}H_3$), 21.4 ($\mathit{C}H_3COOCH_2CH_3$), 61.7 ($CH_3COO\mathit{C}H_2CH_3$) and 172.9 ($CH_3\mathit{C}OOCH_2CH_3$) ppm are assigned to ethyl acetate, the peaks at 18.9 ($\mathit{C}H_3CH_2OH$) and 58.4 ($CH_3\mathit{C}H_2OH$) ppm to ethanol, and the peak at 175.2 ($CH_3\mathit{C}OOH$) to acetic acid. The low-intensity peak of acetic acid at about 20.8 ppm is missing. Noteworthy is that in spite of a relatively high amount of ethyl acetate present in the solution that should generate the same mole quantity of water molecules, this solution (Fe–OAc bond) is very stable against hydrolysis. Figure 9b shows the ^{13}C NMR spectrum of the supernatant of sample AC3 [iron(III) acetate (1.0 g)/ethanol (12.5 mL)/acetic acid (12.5 mL) autoclaved at 180 °C for 24 h]. Ethyl acetate, ethanol and acetic acid were again detected. The relative concentration of ethyl acetate in this supernatant was high because of the proper ratio of ethanol and free acetic acid. Figure 9c shows the ^{13}C NMR spectrum of the supernatant of sample ET3 that contained no added acetic acid. In this NMR spectrum, the peaks of ethanol at δ = 18.7 and 58.1 ppm prevailed; however, all peaks corresponding to ethyl acetate at 14.7, 21.2, 61.3 and 172.3 are also present. The relatively very small intensities of the ethyl acetate peaks are not surprising, because there is a high screening effect due to the presence of an enormous quantity of ethanol. Additionally, the peaks of acetic acid are not visible in this spectrum. The presence of ethyl acetate in this spectrum shows that ester could be formed without the addition of free acetic acid.

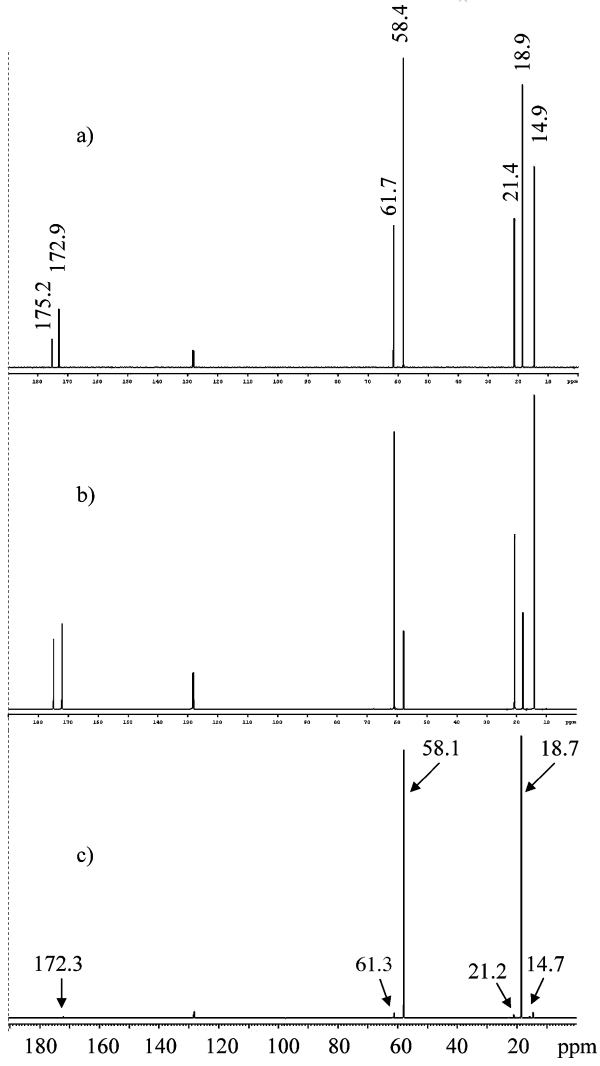

Figure 9. ^{13}C NMR spectrum of (a) a solution containing iron(III) acetate (0.1 g) dissolved in ethanol (17 mL) and acetic acid (33 mL) and aged for 3 months at room temperature, (b) the supernatant of sample AC3 and (c) the supernatant of sample ET3.

In this work, basic iron(III) acetate dissolved in ethanol (octanol) or in an acetic acid/ethanol mixture gave a transparent reddish to very dark reddish solution that was stable at room temperature for months. An attempt to hydrolyse this solution at 90 °C under reflux was not successful. Autoclaving the iron(III) acetate dissolved in absolute ethanol for 8 and 16 h at 180 °C yielded substoichiometric magnetite as a single phase. This result is in accordance with the work of Filho et al.,[7a] who found that magnetite was obtained by heating iron(III) hydroxyacetate under a nitrogen atmosphere. Findings[7b] that the presence of acetate ions had a pronounced reducing effect on the thermal decomposition of iron(II) acetate and iron(III) hydroxy acetate are also in accordance with results of this work. However, the mechanism of solid-state reduction of Fe^{3+} to Fe^{2+} that included the formation of acetone and carbon dioxide differs from that obtained in "wet"-chemistry synthesis.

The mechanism of formation of nanocrystalline iron oxide particles can be explained as follows: basic iron(III) acetate that already contains hydroxy groups is readily soluble in ethanol and octanol and stable in an organic medium, because iron(III) is protected against nucleophilic attack by strong Fe–OAc (OAc = acetate) bonds. However, under more aggressive experimental conditions (autoclaving at 180 °C), ethanol, as a small, polar and very reactive molecule, can easily attack and compete with the acetate groups for the iron sites. The presence of ethanol and iron(III) acetate[8a–8c] can activate various catalytic processes, such as an oxidative dehydrogenation of ethanol to acetaldehyde, acetone or ethyl acetate. For instance, Idriss and Seebauer[8d] found that in the reaction of ethanol over Fe_2O_3, an appreciable amount of ethyl acetate was produced. The authors suggested that ethyl acetate was formed by the Tishchenko reaction, in which the final step included acetate species in proximity of an ethoxide species weakly bonded at the surface of Fe_2O_3. In our system, there is no oxygen to oxidise ethanol; however, the oxidation of ethanol can be induced by the presence of iron(III). Thus, in the oxidative esterification of ethanol into ethyl acetate,

Fe^{3+} can serve as an electron acceptor and be reduced to Fe^{2+}, and magnetite is formed exclusively. Generally, water molecules can be generated by alcohol dehydration in a process concurrent with the esterification reaction. The probability for dehydration of alcohol increases with the number of C atoms. Also, secondary and tertiary alcohols are more reactive than primary alcohols. Thus, the dehydration of ethanol is very difficult, whereas the dehydration process of octanol can occur to some extent, which would result in the production of water molecules. Regardless of the prevailing mechanism, octanol is less polar and a much bigger molecule, and because of that in the iron(III) acetate/octanol system the transfer of electrons to Fe^{3+} is limited, that is, a small quantity of hematite in the precipitate could not be avoided. The possibility that some other catalytic reactions were involved in the hydrolysis of iron(III) acetate/alcohol solutions could not be excluded. With the addition of acetic acid, oxidative conditions prevailed in the system. This is because the free acetic acid, which is not bonded to iron, directly participates in the esterification reaction with ethanol. Water molecules generated in situ in this esterification reaction hydrolyse iron(III) acetate, and hematite is exclusively formed.

It should be noted that the hydroxy groups present in the precursor and the trace amounts of water in the commercial chemicals used in this work participated in the hydrolysis of iron(III) acetate. However, we have clearly shown that bonded acetate in the precursor versus added acetic acid involved in the esterification reaction had a dominant role in tailoring the phase composition of the precipitates.

The synthetic procedure presented in this work is a solvothermal synthesis, which started from homogeneous ethanol or octanol solutions. Like in aqueous media, the early stage of precipitation of iron oxide in ethanol solvents involves nucleation continued with the crystal growth. The primary particles are in the nanometre range, and generally, they show a high tendency to achieve a minimum of the particle's surface energy. The unstable primary particles aggregated in micrometre spherical secondary particles. The spherical shape of the particles is energetically the most probable due to the lowest possible surface-to-volume ratio. Thus, in ethanol solvent, primary nanoparticles aggregated into regular spheres; however, in octanol solvent primary nanoparticles aggregated into large irregular aggregates. This difference in secondary aggregation could be explained by different interactions of the solvent molecules with the surface of the primary particles. Ethanol as a small and polar molecule[9] may contribute in the aggregation with reversible hydrogen bonding between the surfaces of the primary particles. On the contrary, octanol as a much bigger and nonpolar molecule did not show a tendency to form hydrogen bonds. In the case of octanol, van der Waals forces that are much weaker than hydrogen-bonding interactions were involved in the secondary aggregation. These weak forces and the steric hindrance of the long chains of octanol (1.2 nm) favoured the aggregation of primary particles into large irregular aggregates instead of into regular spheres, as in the case of ethanol.

Conclusions

The results relating to the synthesis of nanosized iron oxide particles by using a solvothermal approach with the participation of an esterification reaction in the iron(III)/acetic acid/alcohol system were shown. When basic iron(III) acetate was autoclaved in pure ethanol, magnetite was exclusively formed. In the presence of pure octanol, magnetite was the dominant phase, whereas the formation of hematite could not be avoided. In the presence of ethanol and free acetic acid, exclusively nanosized hematite particles were obtained. The supernatants of the synthesised samples were analysed by ^{13}C NMR spectroscopy, which revealed the presence of ethyl acetate ester in the supernatants.

Various catalytic reactions were activated when basic iron(III) acetate was autoclaved in an organic medium at 180 °C. The formation of ester in the iron(III) acetate/ethanol system was explained by the catalytic oxidation of ethanol in the proximity of acetate groups bonded to iron. In this configuration, the oxidation of ethanol into ethyl acetate was accompanied by a reduction of Fe^{3+} to Fe^{2+}, and magnetite was exclusively formed. Upon the addition of acetic acid to the iron(III) acetate/ethanol system, the free acetic acid directly participated in an esterification reaction with ethanol. Water molecules generated in situ in this esterification reaction hydrolysed iron(III) acetate, and hematite was formed.

In the presence of ethanol, primary nanosized particles aggregated into micrometre regular spheres. Ethanol may contribute in aggregation with reversible hydrogen bonding between the surfaces of the primary particles. Octanol as a nonpolar molecule did not show this tendency. In the case of octanol, van der Waals forces that are much weaker than hydrogen bonds were involved in the secondary aggregation. These weak forces and the steric hindrance of the long chains of octanol (1.2 nm) favoured the aggregation of primary particles into large irregular aggregates instead of into regular spheres, as in the case of ethanol.

Experimental Section

General: Glacial acetic acid [CH_3COOH; Kemika (Zagreb)], absolute ethanol [CH_3CH_2OH; Kemika (Zagreb)] and octanol [$CH_3(CH_2)_7OH$; Aldrich] were of analytical purity and used as received. Anhydrous iron(II) acetate (Aldrich and Across) was analysed by using Mössbauer spectroscopy, and it found that all iron was present as iron(III), that is, the basic iron(III) acetate was formed. Elemental analysis of the Aldrich chemical gave the stoichiometry of $FeC_{4.4}H_{8.8}$.

Typical Procedures: Iron(III) acetate (1.00 g) was dissolved in absolute ethanol, and the solution was then bubbled with N_2 for 20 to 30 min. A clear and dark reddish transparent solution was transferred into a 50-mL Teflon-lined stainless steel autoclave (Parr, model 4744) and heated at 180 °C for 2, 8 and 16 h for samples ET1, ET2 and ET3, respectively. A series of experiments was also performed with iron(III) acetate and octanol for samples OC0 (2 h), OC1(4 h), OC2 (24 h) and OC3 (66 h). Some of the experiments were performed with iron(III) acetate (1.00 g) with the addition of acetic acid (5.0 mL) and ethanol (20 mL); the sample was autoclaved for

2 h (sample AC1). Others involved iron(III) acetate (1.00 g) with the addition of acetic acid (12.5 mL) and ethanol (12.5 mL); the sample was autoclaved for 2 and 24 h at 180 °C (samples AC2 and AC3, respectively).The fourth series of experiments was performed at a much lower concentration of iron(III) acetate (0.1 g), also with the addition of acetic acid (17 mL) and ethanol (33 mL) for samples AD1 and AD2. After autoclaving, the precipitate was washed with absolute ethanol and separated from the supernatant by centrifugation at 15000 rpm for 5–10 min. The isolated precipitate was dried under vacuum at room temperature for 48 h. Dried powder samples were analysed by ^{57}Fe Mössbauer and FE SEM. Supernatants were analysed by ^{13}C NMR spectroscopy. The ^{57}Fe Mössbauer spectra were recorded in the transmission mode by using the standard instrumental configuration by WissEl GmbH (Starnberg, Germany). The ^{57}Co in the rhodium matrix was used as a Mössbauer source. The spectrometer was calibrated at room temperature by using the spectrum of standard α-Fe foil. The velocity scale and all the data refer to the metallic α-Fe absorber at room temperature. The experimentally observed Mössbauer spectra were fitted with the MossWinn program. The XRD patterns were recorded at room temperature by using the APD 2000 X-ray powder diffractometer (Cu-K_α radiation, graphite monochromator, scintillation detector) manufactured by ItalStructures, Riva del Garda, Italy. Rietveld refinements were performed with the MAUD program. The thermal FE SEM (model JSM-7000F) was manufactured by Jeol Ltd. ^{13}C NMR spectra were recorded with a Bruker AV-600 spectrometer, operating at 150.92 MHz. The reference compound used in experiments was TMS (tetramethylsilane).

Acknowledgments

The authors thank Dr. Ž. Marinić for his valuable discussion regarding the results of the NMR spectroscopic analysis. Special thanks to Dr. L. Sekovanić for his critical reading of this manuscript and his valuable suggestions and comments.

[1] a) M. Gotić, S. Musić, M. Ivanda, M. Šoufek, S. Popović, *J. Mol. Struct.* **2005**, *744–747*, 535–540; b) S. Musić, M. Gotić, S. Popović, *Mater. Lett.* **1994**, *20*, 143–148.

[2] a) M. Gotić, M. Ivanda, S. Popović, S. Musić, *Mater. Sci. Eng.* **2000**, *B77*, 193–201; b) S. Ivanković, S. Musić, M. Gotić, N. Ljubešić, *Toxicol. in vitro* **2006**, *20*, 286–294; c) M. Gotić, T. Jurkin, S. Musić, *Colloid Polym. Sci.* **2007**, *285*, 793–800; d) M. Gotić, T. Jurkin, S. Musić, manuscript in preparation; e) M. Gotić, S. Popović, S. Musić, *Mater. Lett.* **2007**, *61*, 709–714.

[3] a) C.-J. Jia, L.-D. Sun, Z.-G. Yan, L.-P. You, F. Luo, X.-D. Han, Y.-C. Pang, Z. Zhang, C.-H. Yan, *Angew. Chem. Int. Ed.* **2005**, *44*, 4328–4333; b) A. Cabañas, M. Poliakoff, *J. Mater. Chem.* **2001**, *11*, 1408–1416; c) M. Gotić, S. Popović, M. Ivanda, S. Musić, *Mater. Lett.* **2003**, *57*, 3186–3192; d) S. Musić, M. Gotić, M. Ivanda, S. Popović, A. Turković, R. Trojko, A. Sekulić, K. Furić, *Mater. Sci. Eng.* **1997**, *B47*, 33–40; e) M. Gotić, M. Ivanda, S. Popović, S. Musić, A. Sekulić, A. Turković, K. Furić, *J. Raman Spectrosc.* **1997**, *28*, 555–558; f) M. Gotić, M. Ivanda, A. Sekulić, S. Musić, S. Popović, A. Turković, K. Furić, *Mater. Lett.* **1996**, *28*, 225–229.

[4] H.-O. Jungk, C. Feldmann, *J. Mater. Res.* **2000**, *15*, 2244–2248.

[5] a) M. Niederberger, G. Garnweitner, *Chem. Eur. J.* **2006**, *12*, 7282–7302; b) Y.-w. Jun, J.-s. Choi, J. Cheon, *Angew. Chem. Int. Ed.* **2006**, *45*, 3414–3439; c) N. Pinna, S. Grancharov, P. Beato, P. Bonville, M. Antonietti, M. Niederberger, *Chem. Mater.* **2005**, *17*, 3044–3049.

[6] a) M. Ivanda, S. Musić, S. Popović, M. Gotić, *J. Mol. Struct.* **1999**, *481*, 645–649; b) N. Šijaković-Vujičić, M. Gotić, S. Musić, M. Ivanda, S. Popović, *J. Sol-Gel Sci. Technol.* **2004**, *30*, 5–19; c) S. Ivanković, M. Gotić, M. Jurin, S. Musić, *J. Sol-Gel Sci. Technol.* **2003**, *27*, 225–233.

[7] a) P. P. de Abreu Filho, E. A. Pinheiro, F. Galembeck, *React. Solids* **1987**, *3*, 241–250; b) S. Musić, M. Ristić, S. Popović, *J. Radioanal. Nucl. Chem. Ar.* **1988**, *121*, 61–71.

[8] a) R. Pestman, R. M. Koster, J. A. Z. Pieterse, V. Ponec, *J. Catal.* **1997**, *168*, 255–264; b) R. Pestman, R. M. Koster, A. van Duijne, J. A. Z. Pieterse, V. Ponec, *J. Catal.* **1997**, *168*, 265–272; c) J. I. Di Cosimo, V. K. Díez, M. Xu, E. Iglesia, C. R. Apesteguía, *J. Catal.* **1998**, *178*, 499–510; d) H. Idriss, E. G. Seebauer, *J. Mol. Catal. A* **2000**, *152*, 201–212.

[9] J. S. Park, H. J. Hah, S. M. Koo, Y. S. Lee, *J. Ceram. Process. Res.* **2006**, *7*, 83–87.

Received: September 15, 2007
Published Online: January 15, 2008

